Synthesis of MoS_2/g-C_3N_4 as a Solar Light-Responsive Photocatalyst for Organic Degradation

Wen-chao Peng and Xiao-yan Li*

Environmental Engineering Research Centre, Department of Civil Engineering,

The University of Hong Kong, Pokfulam, Hong Kong SAR, China

(*Corresponding author: phone: 852 2859-2659; fax: 852 2859-5337; e-mail: xlia@hkucc.hku.hk)

Abstract

Photocatalytic degradation of organic contaminants is an attractive chemical process owing to its potential for using solar light for environmental applications. In this study, a novel molybdenum disulfide (MoS_2) and graphitic carbon nitride (g-C_3N_4) composite photocatalyst was synthesized using a low temperature hydrothermal method. MoS_2 nanoparticles formed on g-C_3N_4 nanosheets in the composite and this MoS_2 incorporation greatly enhanced the photocatalytic activity of g-C_3N_4. The photocatalyst was tested for the degradation of methyl orange (MO) under simulated solar light. Composite 3.0wt% MoS_2/g-C_3N_4 showed the highest photocatalytic activity for MO decomposition. MoS_2 nanoparticles increased the interfacial charge transfer and thus prevented the recombination of photo-generated electron–hole pairs. The new MoS_2/g-C_3N_4 photocatalyst material also displayed good stability during the photo-reactions and the recycled catalyst showed little reduction in activity during repeated test runs. The novel MoS_2/g-C_3N_4 composite is therefore shown as a promising catalyst for photocatalytic degradation of organic pollutants using solar energy.

Key words: Decoloration, graphitic carbon nitride (g-C_3N_4), molybdenum disulfide (MoS_2), photocatalysis, methyl orange, organic degradation

1. Introduction

Much attention has been focused on the photocatalytic strategy for the removal of environmental contaminants, as solar energy is an inexhaustible and environmentally friendly energy resource.[1] A large number of semiconductor materials, such as metal oxides and metal sulfides (e.g. TiO_2 ,WO_3, CdS, ZnS and ZnO), have been developed as active catalysts for photocatalysis of organic pollutants.[2] Efforts have been made in recent years to use non-metal materials in the synthesis of new photocatalysts with improved reactivity and stability.[3] Wang et al. reported a novel polymeric photocatalyst, graphitic carbon nitride (g-C_3N_4) that exhibits excellent photocatalytic hydrogen production using solar energy.[4] The metal-free g-C_3N_4 photocatalyst possesses a good electronic property as well as a high thermal and chemical stability, making it a valuable material for photocatalytic applications.[1, 5, 6] However, the photocatalytic efficiency of bare g-C_3N_4 is still limited due to the high rate of recombination of the photo-generated electron–hole pairs.[7] For further improvement, co-catalyst materials, including noble metals, semiconductors and carbon allotropes, have been combined with g-C_3N_4 to fabricate new composite photocatalysts.[1, 7-14]

It is well known that loading precious metals, such as Pt and Au, effectively enhances the activity of photocatalysts. However, these metals are rare and expensive to apply. Molybdenum disulfide (MoS_2) is an emerging photocatalytic cocatalyst material that may be used as a substitute for noble metals in synthesizing photocatalysts. As an indirect-gap semiconductor, MoS_2 has a rather narrow band gap (1.29 eV), and its conduction band (CB) and valence band (VB) edge potentials (-0.1 and +2.0 eV) are more positive than most photosensitive semiconductors.[8, 9] The difference between the CB edge potentials of a semiconductor and MoS_2 allows electron transfer from the semiconductor to MoS_2, which would make the CB electrons more mobile and hence promote the separation of electron-hole pairs on the semiconductor.[8, 10] Metal oxides and metal sulfates show improved

photocatalytic activity when MoS_2 is added as a synergistic cocatalyst.[11, 12] Recently, a g-C_3N_4-MoS_2 composite was synthesized by mixing g-C_3N_4 and MoS_2 together, which was found to be effective for photocatalytic H_2 generation.[10] In this study, we prepared the g-C_3N_4-MoS_2 composites using a facial low temperature hydrothermal method to deposit MoS_2 as nanoparticles on the g-C_3N_4 sheets. The resulting composite catalyst exhibited a high photocatalytic activity and good stability for the degradation of methyl orange under simulated solar light.

2. Experimental

2.1 Synthesis of g-C_3N_4 from thiourea

Ten grams of thiourea powder was put into an alumina crucible with a cover that was placed in a tube furnace. The chemical was heated to 550 ^oC at a heating rate of 10 ^oC /min and kept at this temperature for 2 h in air. The air exhaust released during the thermal treatment was absorbed by a dilute NaOH solution (0.05 M). The resulting yellow powder collected was g-C_3N_4.[13]

2.2 Synthesis of g-C_3N_4 supported MoS_2 nanoparticles

Half a gram prepared g-C_3N_4 was dispersed with sonication in 100 mL DI water with ammonium molybdate ($(NH_4)_6Mo_7O_{24}\cdot 4H_2O$) and $Na_2S\cdot 4H_2O$. The mixture was stirred for 2 h to obtain a homogeneous solution. Ten mL 35% HCl solution was added and the solution was heated to 90 ^oC. After 30 min, 1 g $NH_2OH\cdot HCl$ was added and the solution was kept at this temperature for another 4 h to grow MoS_2 on g-C_3N_4.[14] The composite, g-C_3N_4-MoS_2, was washed thoroughly with DI water and then dried in an oven at 60^oC for 12 h.

2.3 Photocatalytic degradation of methyl orange

Methyl orange (MO), one of important classes of commercial dyes, was selected as a model chemical compound for photocatalytic experiments. Given the short life of its excited-state and its high stability under visible and near UV irradiation, MO has often been used as a model dye for testing photo-redox reactions that result in color reduction. For a typical MO decomposition test, 50 mg of the photocatalyst powder was first dispersed in 50 mL of water in a quartz photo-tube by sonication, followed by the addition of MO to an initial concentration of 20 mg/L. Before exposure to light, the suspension was stirred in the dark for 10 h to allow adsorption of MO by the catalyst. Photocatalysis of MO was performed in an XPA-7 photo-reactor (Xujiang Electromechanical Plant, Nanjing, China) with a 500 W xenon lamp for the simulated solar (SS) light. During the photocatalytic test, 3 mL of the solution was sampled from the photo-tube at regular time intervals to measure the MO concentration. Each sample was filtered and its absorbance (ABS) was measured by a UV-visible spectrophotometer (UV-vis lambda 25, Perkin Elmer) at 463 nm to determine the MO concentration in the solution.

2.4 Material characterization

The crystal forms of the photocatalysts were analyzed from their X-ray diffraction (XRD) patterns using a Bruker D8 Advance X-ray powder diffractometer. The morphology of the catalysts was examined by transmission electron microscopy (TEM) (Philips Tecnai G220 S-TWIN, Amsterdam, the Netherlands). Fourier transform infrared spectroscopy (FT-IR) (Perkin Elmer, FT-IR Spectrophoeometer Spectrum One B) was used to characterize the functional groups of different catalysts. The chemical states of MoS_2 nanoparticles were detected by X-ray photo-emission spectroscopy (XPS) (PHI 5600 Multi-Technique XPS System, Physical Electronics). The UV-vis diffusive reflectance spectra (DRS) of the catalyst powders were recorded by a spectrophotometer (Hitachi U-3010). The surface area and pore structure of catalyst powder samples was determined by a Beckman Coulter

SA3100 surface area analyzer from the nitrogen adsorption-desorption isotherm at liquid nitrogen temperature (77 K).

3. Results and Discussion

3.1 Characterization of the photocatalysts

The commonly used precursors for g-C_3N_4 are nitrogen rich compounds with a pre-bonded triple or double C–N core structure, such as cyanamide and dicyandiamide, which are unstable, highly explosive and toxic. In this study, a low cost, non-toxic chemical, thiourea, was used as the raw material to produce g-C_3N_4. The process is simple and easy to perform and can be completed in 2 h at 550 ^oC in the air atmosphere. MoS_2 nanoparticles were formed and deposited on g-C_3N_4 by the reduction of molybdate with $NH_2OH{\cdot}HCl$ at 90 ^oC. The reaction mechanisms for this process can be described as follows:

$$(NH_4)_6Mo_7O_{24} + Na_2S \xrightarrow{HCl} (NH_4)_2MoS_4 \xrightarrow{NH_2OH\cdot HCl} MoS_2$$

The composite sample was first characterized by XPS to verify its chemical composition. As shown in Fig. S1a, the Mo3d spectrum exhibits two peaks at 229.4 eV ($Mo3d_{5/2}$) and 232.4 eV ($Mo3d_{3/2}$), indicating a +4 oxidation state for Mo in the composite. The peak at 163.2 eV in Fig. S1b can be attributed to S2p of S^{2-}. These binding energies are all close to the reported values for MoS_2.[10, 15-17]

Fig. 1 presents the XRD patterns of the g-C_3N_4 and g-C_3N_4-MoS_2 samples. The g-C_3N_4 spectra show a strong peak at 27.4^o corresponding to the tight inter-layer stacking distance (0.325 nm) of the aromatic planes in g-C_3N_4. The other pronounced peak at 13.11^o corresponds to an in-plane structural repeating motif with a repeated distance of 0.675 nm. Pure MoS_2 nanoparticles were prepared using the same method as described for the

120 composite, without the addition of g-C_3N_4. As shown in Fig. 1, the XRD profile for pure
121 MoS_2 displayed low and broad diffraction peaks. The pattern of broad peaks was likely
122 caused by the combination of small-size particles, disorder in crystallinity and strains in the
123 crystallites.[16] The XRD pattern for g-C_3N_4-MoS_2 is nearly the same as that for g-C_3N_4, due to
124 the small percentage of MoS_2 and its low diffraction intensity. The FT-IR spectra also show
125 little difference between pure g-C_3N_4 and g-C_3N_4-MoS_2 (Fig. S2).

126 **Fig. 1.**

127 The optical absorption property of g-C_3N_4-MoS_2 composites with various MoS_2 contents
128 was analyzed. According to the DRS in Fig. 2, pure g-C_3N_4 displays absorption from UV
129 through the visible range up to 460 nm, which can be ascribed to the band gap of g-C_3N_4 (2.7
130 eV). In the UV (≤400 nm) region, the composites' absorption abilities follows the order g-
131 C_3N_4-0.03MoS_2 > g-C_3N_4-0.05MoS_2 > g-C_3N_4-0.01MoS_2 > g-C_3N_4. Generally, in the low
132 energy visible region, the DRS intensity strengthened with an increase of the MoS_2 content in
133 the g-C_3N_4-MoS_2 composite. The differences in optical adsorption agree well with the colors
134 of the catalyst powders, presented in Fig. 2, which range from yellow to brown. The DRS
135 features suggest that MoS_2 doping can enhance the response of the catalyst composite
136 towards solar light.

137 **Fig. 2.**

138 The TEM image of g-C_3N_4 in Fig. 3a shows a clear nanosheet structure similar to
139 graphene. The nanosheets are very thin and transparent to the electron beam. The TEM image
140 of pure MoS_2 in Fig. 3b shows aggregated nanoparticles in a wide size distribution. At a
141 higher magnification in Fig. 3c, a relatively weak crystallinity and strain of the MoS_2 in the
142 crystallites can be observed. The characteristic crystal lattice of MoS_2 (0.62 nm) can be
143 identified at the edge of the nanoparticles. The morphology and microstructure of the g-C_3N_4-

144 MoS_2 composite are shown in detail in the TEM image in Fig. 3d. MoS_2 nanoparticles on the
145 g-C_3N_4 surface can be seen at the edge of the composite, and the MoS_2 deposition does not
146 appear to disrupt the g-C_3N_4 nanosheets.

147 **Fig. 3.**

148 The specific surface area and pore volume of the catalyst samples were measured using
149 nitrogen adsorption (Fig. S3). The g-C_3N_4-MoS_2 composites have a larger surface area than
150 g-C_3N_4 (17.5 m^2/g), but there is little difference between the composites with different MoS_2
151 loading percentages. The N_2 adsorption-desorption isotherms in Fig. S3a indicate that g-
152 C_3N_4-0.03MoS_2 has a greater N_2 adsorption capability than pure g-C_3N_4. The diameter of the
153 main pores increased with the MoS_2 content, from 18 nm for g-C_3N_4 to 30 nm for g-C_3N_4-
154 0.03MoS_2 (Fig. S3b), which is likely to be the cause of the composite's increased surface area.

155 **3.2 Photocatalytic decomposition of methyl orange**

156 The photocatalytic activity of the different catalysts was tested by the decoloring or
157 decomposition of 20 mg/L MO under simulated solar light. Prior to the photo-tests, the
158 changes in MO concentration caused by the adsorption of the catalyst materials were
159 determined in the dark. The adsorption capability of g-C_3N_4 clearly increased with MoS_2
160 deposition (Fig. S4). This is attributable to the increases in the surface area and pore size of
161 the composites (Fig. S3). After adsorption, the equilibrium MO concentrations were used as
162 the initial concentrations for the subsequent photocatalysis tests (Fig. 4). Composite g-C_3N_4-
163 MoS_2 exhibited a much greater photocatalytic activity than bare g-C_3N_4 for MO destruction.
164 The photocatalytic efficiency for MO decoloration under SS light follows the order g-C_3N_4-
165 0.03MoS_2 > g-C_3N_4-0.05MoS_2 > g-C_3N_4-0.01MoS_2 > g-C_3N_4. Integration of 1% MoS_2 into g-
166 C_3N_4 greatly increased its photocatalytic activity. Increase of the MoS_2 doping ratio to 3%
167 further increased the activity of the photocatalyst. However, when the MoS_2 ratio increased to

168 5%, the photo-activity of the catalyst decreased according to the MO degradation tests. The
169 half-time ($T_{1/2}$) of MO decoloring by the photocatalysts can be determined from the MO
170 reduction curves. Under SS light, the $T_{1/2}$ of MO for bare g-C_3N_4 was 1253 min, whereas the
171 $T_{1/2}$ for g-C_3N_4-0.03MoS_2 was only 213 min.

172 **Fig. 4.**

173 An unsuccessful attempt was made to further increase the activity of the photocatalyst by
174 annealing the g-C_3N_4-0.03MoS_2 composite at different temperatures. The photo-activity of
175 the catalyst actually decreased after the annealing treatment; even at the maximum annealing
176 temperature of 400 ^oC (g-C_3N_4 becomes unstable at 400 ^oC or higher). Detailed experiment
177 and results are reported in the Supporting Information (Fig. S5).

178 The stability of the g-C_3N_4-0.03MoS_2 composite as a photocatalyst was evaluated by
179 repeating the MO decoloration tests. As shown in Fig. S6, the adsorption capacity of g-C_3N_4-
180 0.03MoS_2 decreased after the first use, but little further decrease was observed in the
181 following test runs. The photo-activity of the catalyst was stable, as indicated by the repeated
182 MO decoloring tests (Fig. 5). No significant deactivation was found for the recycled
183 photocatalyst after four runs.

184 **Fig. 5.**

185 **3.3 Photocatalytic MO degradation mechanisms by g-C_3N_4-MoS_2**

186 The mechanisms of photocatalytic MO degradation by the g-C_3N_4-MoS_2 composite are
187 illustrated in Fig. 6. MO molecules are readily adsorbed via conjugation by the s-triazine
188 rings (C_3N_3) of g-C_3N_4, which is beneficial to the subsequent MO decomposition. Under SS
189 light, irradiation of photosensitive g-C_3N_4 leads to electron excitation and electron–hole pair
190 formation. The CB and VB edge potentials of polymeric g-C_3N_4 are reported at -1.13 and
191 +1.57 eV [8]. In comparison, the CB and VB edge potentials of MoS_2 are more positive, at -0.1

and +2.0 eV. The difference between the CB edge potentials of g-C_3N_4 and MoS_2 allows electron transfer from the CB of g-C_3N_4 to the CB of MoS_2, which is favorable to the separation of electron-hole pairs on g-C_3N_4.[8, 10] Therefore, MoS_2 nanoparticles on the g-C_3N_4 sheets apparently act as electron collectors, similarly to noble metals, conducting photo-generated electrons from the main photocatalyst and thus preventing the electrons from recombining with the holes. Moreover, the presence of MoS_2 could provide more active sites for MO adsorption and degradation. The electrons would eventually be accepted by dissolved oxygen in the aqueous phase to facilitate the electron–hole separation. The holes can directly oxidize MO molecules adsorbed on the catalyst surface, resulting in color reduction. Moreover, the holes react with water (or hydroxyl) to form hydroxyl free radicals (·OH), which are a strong oxidant for MO decomposition [2, 18][2, 18]. The MO degradation in water results in decoloration of the solution and formation of CO_2 and intermediate products, such as phenolic compounds and carboxylic acids. The major reaction steps during the photocatalytic process may be described by the following equations (1–6):

$$\text{g-}C_3N_4 + h\nu \rightarrow \text{g-}C_3N_4\,(e^- + h^+) \quad (1)$$

$$\text{g-}C_3N_4\,(e^-) + MoS_2 \rightarrow \text{g-}C_3N_4 + MoS_2\,(e^-) \quad (2)$$

$$MoS_2\,(e^-) + 1/2O_2 \rightarrow MoS_2 + O_2^- \quad (3)$$

$$\text{g-}C_3N_4\,(h^+) + MO \rightarrow CO_2 + H_2O + \text{other products} \quad (4)$$

$$\text{g-}C_3N_4\,(h^+) + OH^- \rightarrow \text{g-}C_3N_4 + \cdot OH \quad (5)$$

$$\cdot OH + MO \rightarrow CO_2 + H_2O + \text{other products} \quad (6)$$

Fig. 6.

4. Conclusions

Novel g-C_3N_4-MoS_2 composite photocatalysts were prepared using a facile, low temperature hydrothermal method, with MoS_2 formed as nanoparticles on the g-C_3N_4 nanosheets. The composite catalysts exhibited much greater photocatalytic activity than pure g-C_3N_4 for the decoloration and degradation of methyl orange under simulated solar light, and the 3.0wt% MoS_2/g-C_3N_4 composite had the greatest activity. An annealing process failed to further increase the activity of the photocatalysts. The enhanced photocatalytic activity can be attributed to the synergetic function of MoS_2 in the composite catalyst. The presence of MoS_2 nanoparticles apparently increased the interfacial charge transfer and thus reduced electron–hole recombination. The photocatalyst also displayed good stability during the photo-reactions and no obvious deactivation was found for the recycled catalyst after four test runs. The MoS_2/g-C_3N_4 composite is thus a promising photocatalyst with a high reactivity and stability for photocatalytic degradation of organic pollutants using solar energy.

Acknowledgements

This research was supported by grants HKU714112E from the Research Grants Council (RGC) and SEG_HKU10 from the University Grants Committee (UGC) of the Government of Hong Kong SAR. The technical assistance of Mr. Keith C.H. Wong is highly appreciated.

References

1. W. Liu, M. L. Wang, C. X. Xu and S. F. Chen, *Chem Eng J*, 2012, **209**, 386-393.
2. Q. J. Xiang, J. G. Yu and M. Jaroniec, *Chem Soc Rev*, 2012, **41**, 782-796.
3. G. Liu, P. Niu, L. C. Yin and H. M. Cheng, *J Am Chem Soc*, 2012, **134**, 9070-9073.

4. X. C. Wang, K. Maeda, A. Thomas, K. Takanabe, G. Xin, J. M. Carlsson, K. Domen and M. Antonietti, *Nat Mater*, 2009, **8**, 76-80.
5. Y. Wang, X. C. Wang and M. Antonietti, *Angew Chem Int Edit*, 2012, **51**, 68-89.
6. Y. Zheng, J. Liu, J. Liang, M. Jaroniec and S. Z. Qiao, *Energ Environ Sci*, 2012, **5**, 6717-6731.
7. G. Z. Liao, S. Chen, X. Quan, H. T. Yu and H. M. Zhao, *J Mater Chem*, 2012, **22**, 2721-2726.
8. L. Ge, C. Han and J. Liu, *Applied Catalysis B: Environmental*, 2011, **108**, 100-107.
9. K. F. Mak, C. Lee, J. Hone, J. Shan and T. F. Heinz, *Phys Rev Lett*, 2010, **105**.
10. L. Ge, C. C. Han, X. L. Xiao and L. L. Guo, *Int J Hydrogen Energ*, 2013, **38**, 6960-6969.
11. K. H. Hu, X. G. Hu, Y. F. Xu and J. D. Sun, *J Mater Sci*, 2010, **45**, 2640-2648.
12. X. Zong, H. J. Yan, G. P. Wu, G. J. Ma, F. Y. Wen, L. Wang and C. Li, *J Am Chem Soc*, 2008, **130**, 7176-+.
13. F. Dong, Y. J. Sun, L. W. Wu, M. Fu and Z. B. Wu, *Catal Sci Technol*, 2012, **2**, 1332-1335.
14. Y. M. Tian, J. Z. Zhao, W. Y. Fu, Y. H. Liu, Y. Z. Zhu and Z. C. Wang, *Mater Lett*, 2005, **59**, 3452-3455.
15. H. T. Lin, X. Y. Chen, H. L. Li, M. Yang and Y. X. Qi, *Mater Lett*, 2010, **64**, 1748-1750.
16. X. L. Li and Y. D. Li, *J Phys Chem B*, 2004, **108**, 13893-13900.
17. X. M. Shuai and W. Z. Shen, *J Phys Chem C*, 2011, **115**, 6415-6422.
18. J. C. Liu, H. W. Bai, Y. J. Wang, Z. Y. Liu, X. W. Zhang and D. D. Sun, *Adv Funct Mater*, 2010, **20**, 4175-4181.

Figure Captures

Fig. 1. XRD patterns of pure MoS_2, pure g-C_3N_4 and the g-C_3N_4-MoS_2 composite

Fig. 2. UV-vis diffusive reflectance spectra of g-C_3N_4 and g-C_3N_4-MoS_2 composites.

Fig. 3. (a) TEM image of pure g-C_3N_4, (b) TEM images of pure MoS_2, (c) HR-TEM images of pure MoS_2 and (d) TEM image of g-C_3N_4-MoS_2 composite.

Fig. 4. Degradation of MO under simulated solar light by pure g-C_3N_4 and the g-C_3N_4-MoS_2 composites.

Fig. 5. Photocatalytic MO degradation by the recycled photocatalysts in repeated test runs.

Fig. 6. Schematics of the mechanisms of photocatalytic MO degradation by the g-C_3N_4-MoS_2 composite under SS light.

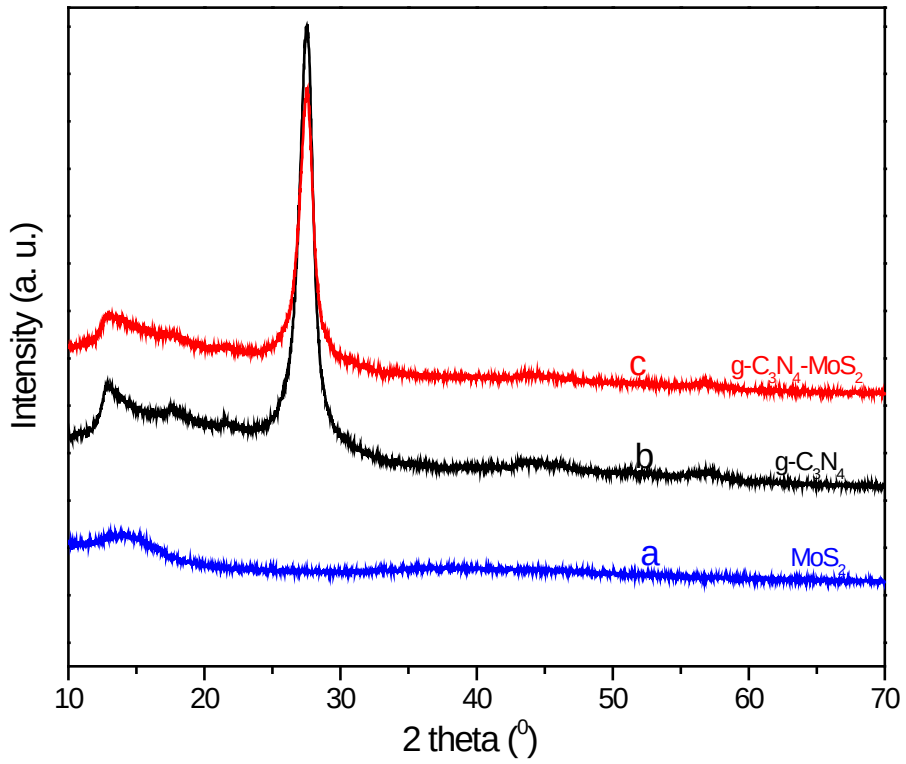

Fig. 1. XRD patterns of pure MoS_2, pure g-C_3N_4 and the g-C_3N_4-MoS_2 composite

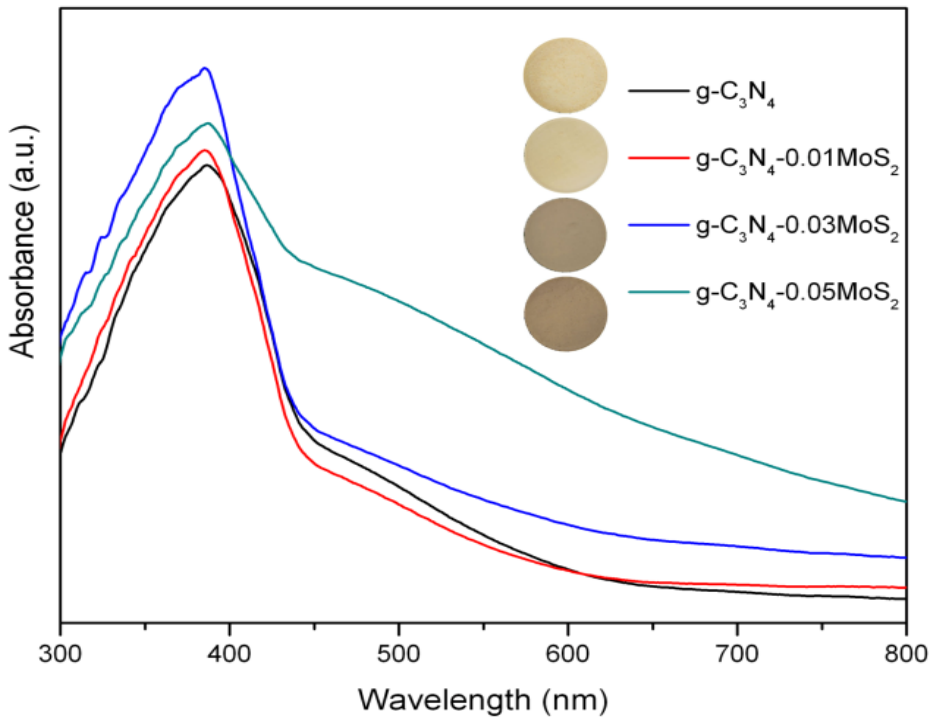

Fig. 2. UV-vis diffusive reflectance spectra of g-C_3N_4 and g-C_3N_4-MoS_2 composites.

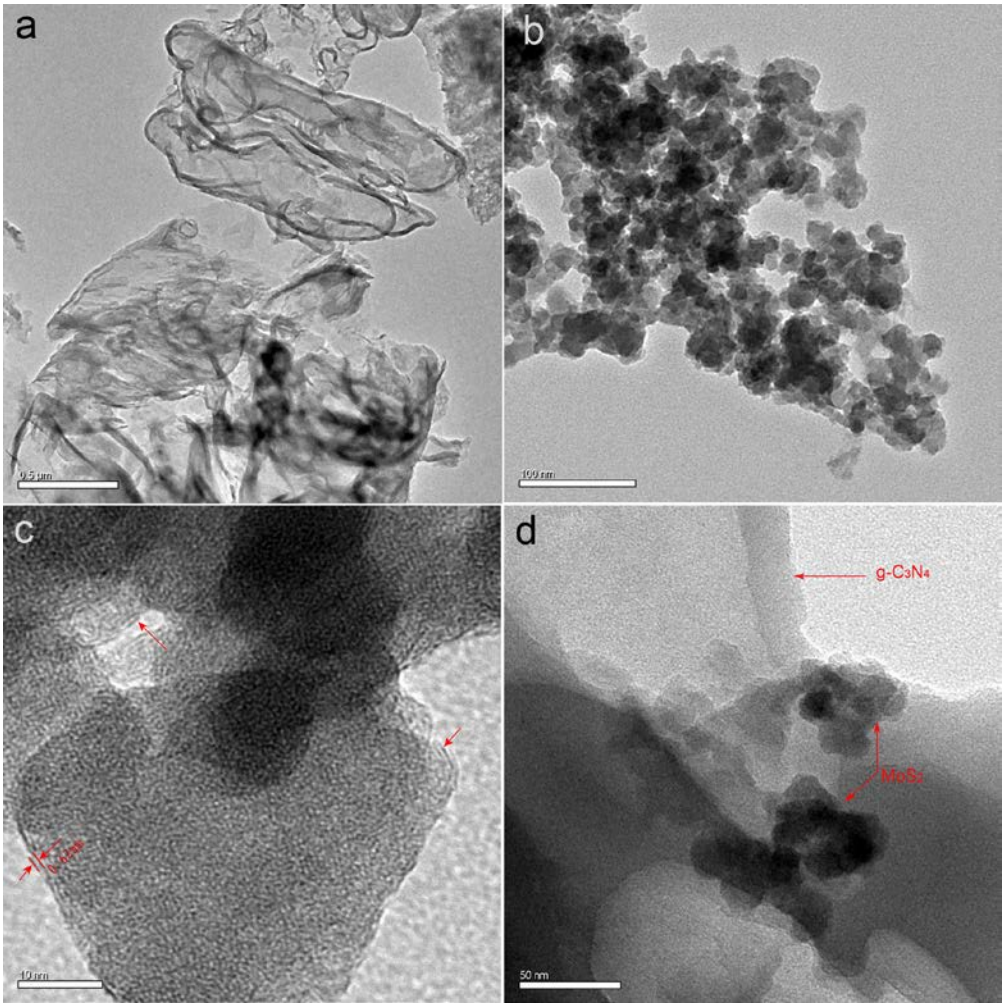

Fig. 3. (a) TEM image of pure g-C_3N_4, (b) TEM images of pure MoS_2, (c) HR-TEM images of pure MoS_2 and (d) TEM image of g-C_3N_4-MoS_2 composite.

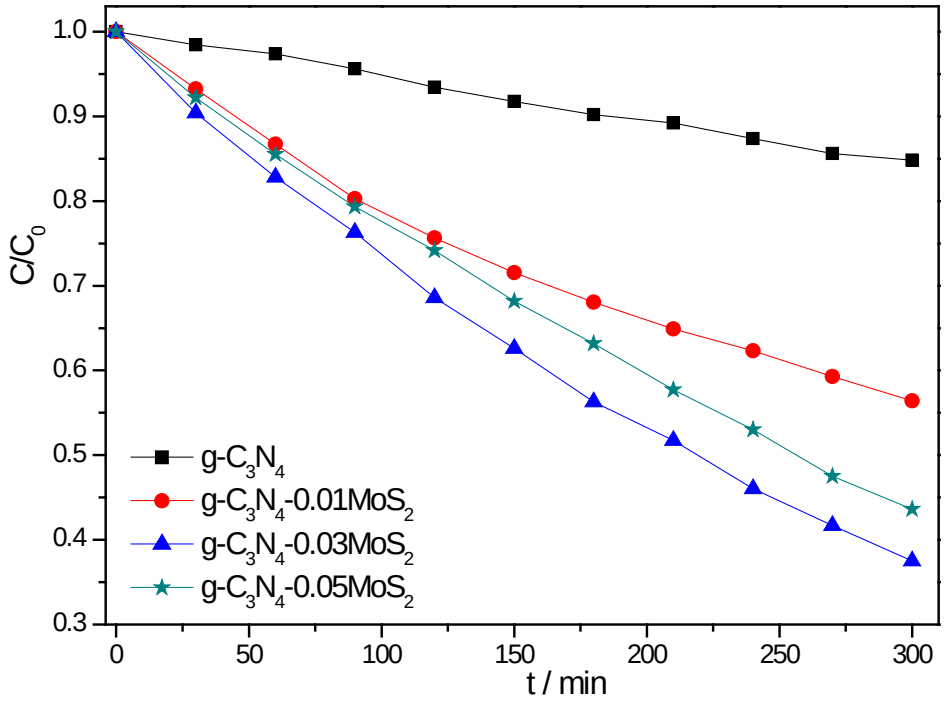

Fig. 4. Degradation of MO under simulated solar light by pure g-C_3N_4 and the g-C_3N_4-MoS_2 composites.

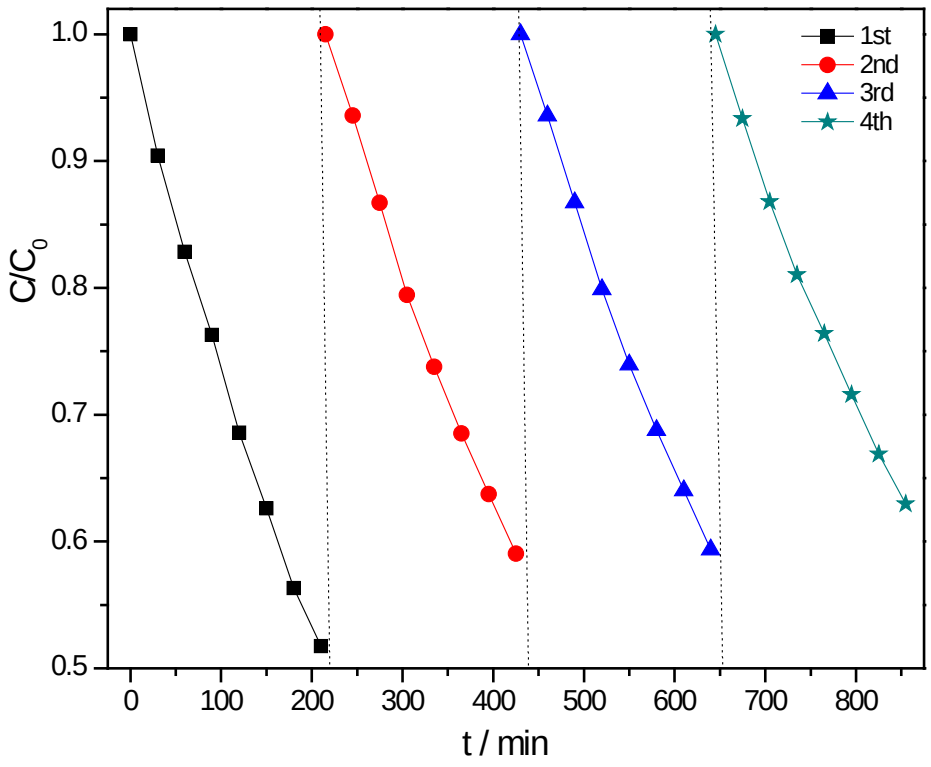

Fig. 5. Photocatalytic MO degradation by the recycled photocatalysts in repeated test runs.

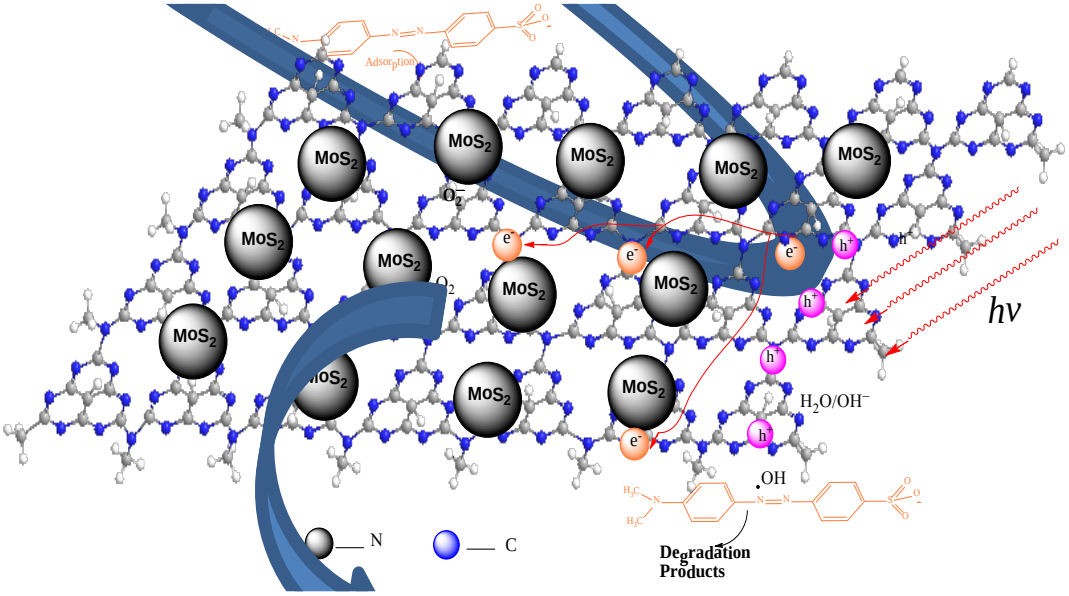

Fig. 6. Schematics of the mechanisms of photocatalytic MO degradation by the g-C_3N_4-MoS_2 composite under SS light.

Supporting Information

Synthesis of MoS_2/g-C_3N_4 as a Solar Light-Responsive Photocatalyst for Organic Degradation

Wen-chao Peng and Xiao-yan Li*

Environmental Engineering Research Centre, Department of Civil Engineering,

The University of Hong Kong, Pokfulam, Hong Kong SAR, China

(*Corresponding author: phone: 852 2859-2659; fax: 852 2859-5337; e-mail: xlia@hkucc.hku.hk)

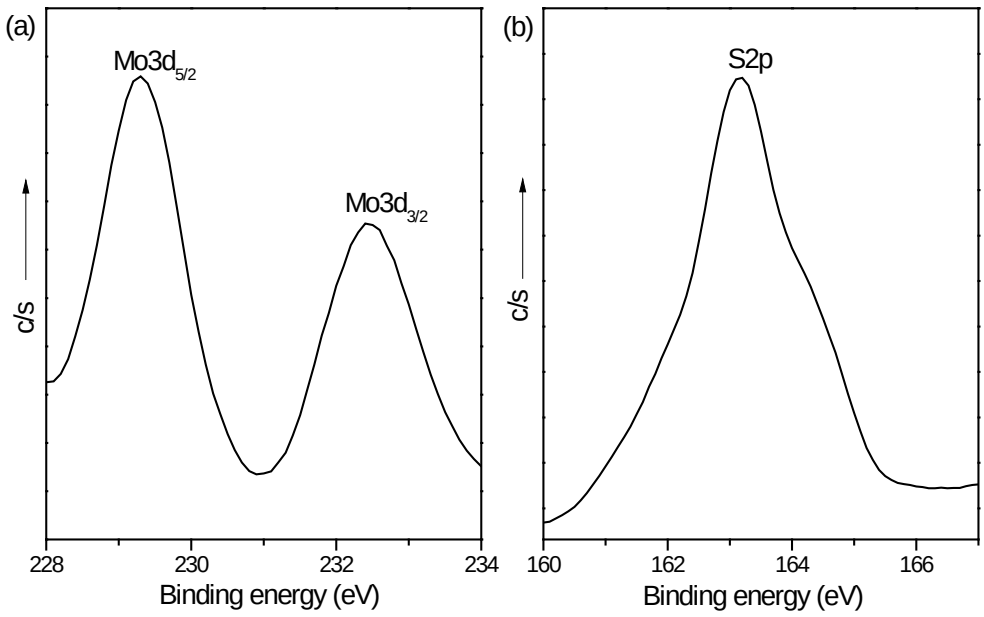

Fig. S1. XPS spectra of MoS_2 nanoparticles deposited on g-C_3N_4: (a) Mo (3d) spectrum and (b) S (2p) spectrum.

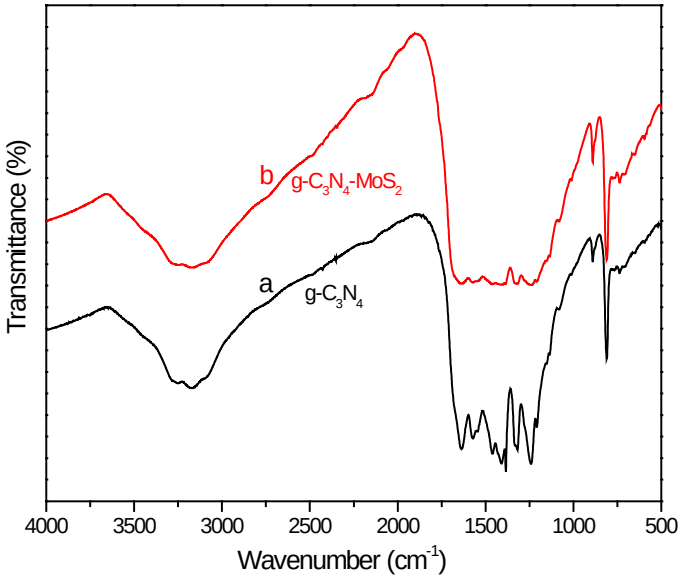

Fig. S2. FT-IR profiles of pure g-C_3N_4 and the g-C_3N_4-MoS_2 composite.

The FT-IR spectrum of pure g-C_3N_4 clearly shows several peaks at the frequency characteristic of the vibrational modes related to the chemical bonding between carbon and nitrogen. The adsorption peak at 810 cm^{-1} corresponds to the breathing mode of the triazine units. Several strong bands in the 1240-1645 cm^{-1} region can be attributed to the stretching modes of C-N heterocyclics (e.g. 1321 cm^{-1} C-N stretching and 1641 C=N cm^{-1} stretching). The broad absorption band at ~3200 cm^{-1} can be assigned to the stretching modes of secondary and primary amines and their intermolecular hydrogen-bonding interactions. No major differences can be seen between the pure g-C_3N_4 and the g-C_3N_4-MoS_2 composite spectra. Therefore, MoS_2 doping did not change the functional groups of g-C_3N_4 and no new chemical bonds were generated during this process. However, the intensity of the peaks (1100-1750 cm^{-1}) for the g-C_3N_4-MoS_2 composite is relatively lower than those of pure g-C_3N_4. This was likely caused by the layer of MoS_2 on the g-C_3N_4 surface, which decreased the transmittance of infrared rays from g-C_3N_4.

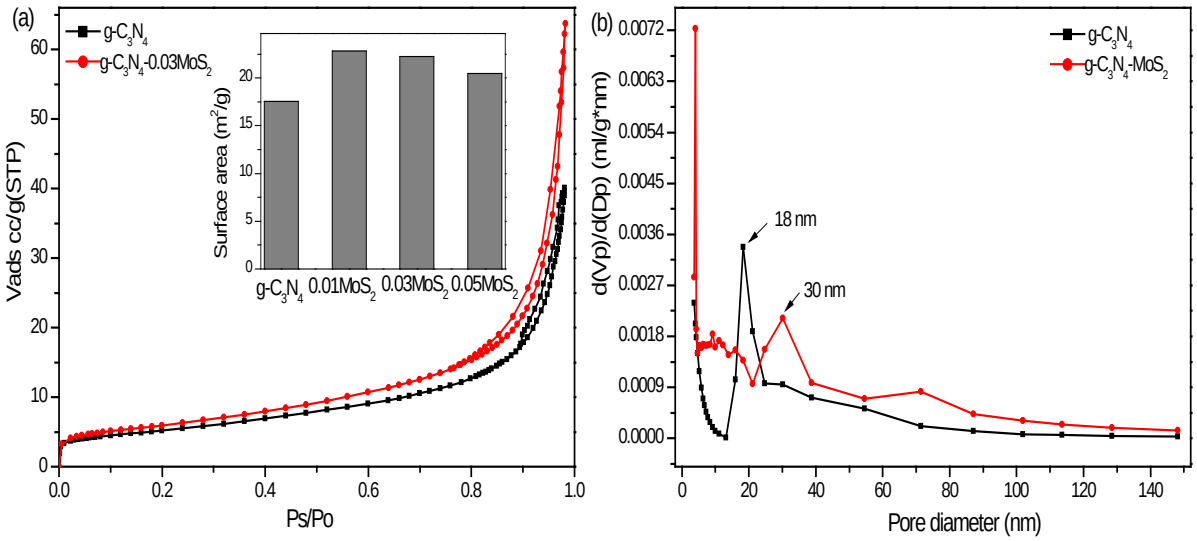

Fig. S3. (a) N_2 adsorption-desorption isotherms at 77 K and (b) pore size distributions of g-C_3N_4 and g-C_3N_4-MoS_2.

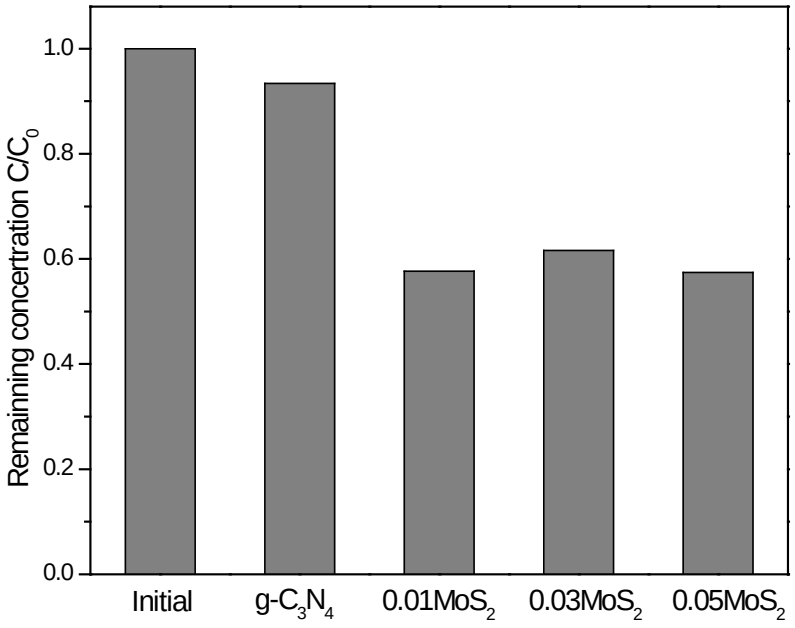

Fig. S4. Change in MO concentration after adsorption by the different catalyst materials ($g\text{-}C_3N_4$ and its composites with different amounts of MoS_2)

Thermal treatment of MoS_2/g-C_3N_4

The g-C_3N_4-0.03MoS_2 composite was placed in a crucible that was placed in a tube furnace. An N_2 flow (50 mL/min) was applied for 2 h to remove air from the furnace. The temperature was increased at a rate of 5 ^oC/min to the required temperature (200, 300 or 400 ^oC) and then maintained at that temperature for 2 h. A temperature higher than 400 ^oC will break the structure of g-C_3N_4, so this was set as the upper temperature limit. The furnace was cooled down naturally to room temperature to complete the annealing process.

The materials obtained were characterized by XRD and the results are shown in Fig. S5a. No major differences can be seen between the different samples. The catalysts were tested for photocatalytic MO degradation under the same conditions. Fig. S5b shows that their adsorption capacity decreased after the annealing treatment. In addition, the photo-activity of the thermally treated catalyst did not show any increase for MO degradation (Fig. S5c). The annealing process therefore did not enhance the photocatalytic activity of g-C_3N_4-0.03MoS_2.

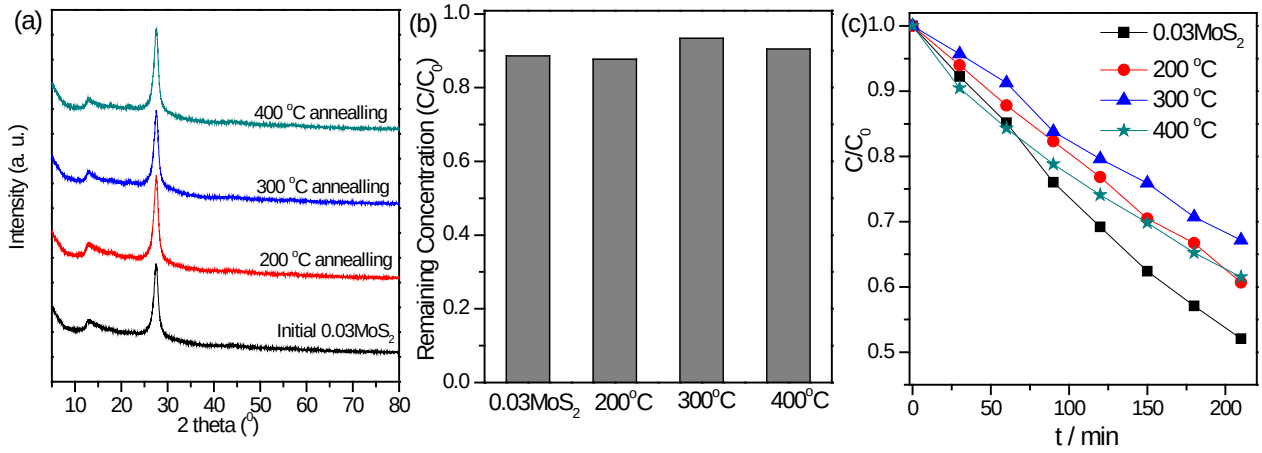

Fig. S5 (a) XRD patterns of g-C_3N_4-0.03MoS_2 annealed at different temperatures in the N_2 atmosphere, (b) the adsorption capability of the different catalyst materials and (c) photocatalytic degradation of MO by the different photocatalysts.

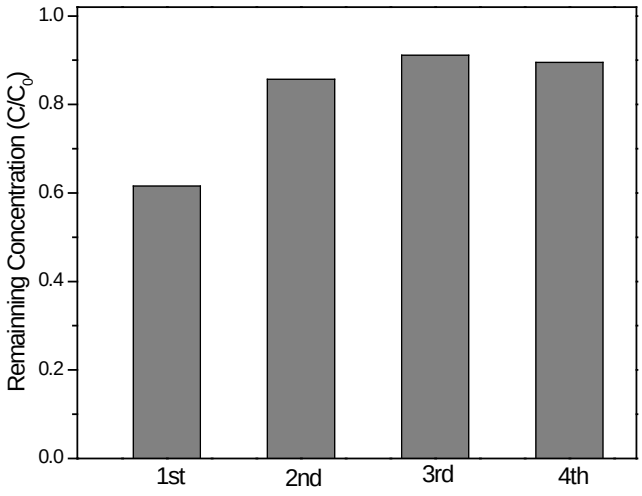

Fig. S6. The adsorption capacity of the recycled catalyst materials